
Chapter 4. Synthesis and study the effect of Mo doping on the structural and dielectric properties of Co-Zn ferrite

4.1 Introduction

In most recent couple of decades, multiferroic materials have pulled in numerous scientists because of its captivating physical properties. The multiferroic materials show both ferromagnetic (FM) and ferroelectric (FE) properties in a solitary phase which make these materials mechanically imperative [196]. Because of the conjunction of both the ordering, it can be utilized to develop high-density memory gadget in which information can be composed magnetically and perused electrically and the other way around [66, 197]. They have additionally some potential applications in magnetic sensors, transducers, spintronics, microwave electronics, phase shifter, resonators, waveguides and spin-wave generator etc. [68, 74, 155, 198, 199]. Multiferroic materials likewise show magneto-electric effect (ME) which by and large alludes the tunable electrical properties when there is an non-zero external magnetic field and the other way around [56, 80, 200].

Cobalt ferrite is a feeble multiferroic material because of the presence of weak ferroelectric ordering in the material [66]. The doping in the A-site of the cobalt ferrite with diamagnetic Zn^{2+} ion strikingly expands the saturation magnetization. The cobalt-zinc ferrite have the general chemical formula $Co_xZn_{1-x}Fe_2O_4$ with inverse spinel structure. The

material likewise has great magnetic, electrical and dielectric properties. Because of the momentous properties of Co-Zn ferrite, for example, high coercivity, large magneto-crystalline anisotropy, low eddy current loss, high electrical resistivity, moderate saturation magnetization, high dielectric constant, low assembling cost, chemical stability and so on [201, 202] they have adaptable applications like antenna cores, satellite communication, coolant, high frequency device, ferrofluids, magnetic switches, biosensor, chemical drug delivery, crystal photonics, transformer cores, read/write head of high speed digital tapes, hyperthermia for cancer treatment, gas sensor, magneto-caloric refrigeration, photo catalysis and contrast enhancer in MRI (Magnetic Resonance Imaging) and so forth. [203-207]. RADER engrossing paint containing ferrite can be utilized for stealth activity by covering on military airship [208]. As of late ferrites have been found to have their potential application as an anode material in Li-ion batteries and solid-oxide fuel cell [62, 72]. The electrical and dielectric properties of ferrites rely upon a few factors, for example, synthesis procedure, structural distortion, dopant and sintering temperature and so on. [65]. Other than a few kinds of synthesis procedures, solid-state reaction procedure is sensibly great to create bulk ferrite material [60, 70, 71, 209, 210]. The behaviors of ferrite material significantly alter when fractional substitution is made by some transition metal or rare earth elements in the iron site of Co-Zn ferrite.

So many research groups have explored the impact of doping with an alternate cation to enhance diverse properties of cobalt ferrite. Vaithyanathan et al. [155] reported the dielectric relaxation properties of Ti-doped cobalt ferrite. The grain and grain boundary contribution in the conduction in cobalt ferrite have been accounted by Kolekar et al. [58].

Rahman et al. [62] demonstrated the improvement of dielectric constant in Gd-doped cobalt ferrite. Dwivedi et al. [66] reported the ferroelectric ordering in Mo-doped Co ferrite in detail. The progressions of dielectric constant with sintering temperature for Dysprosium doped cobalt ferrite nanoparticles have been reported by Kumar et al. [68].

In this chapter, we have incorporated Mo-doped Co-Zn ferrite and concentrated the impact of Mo doping in structural, dielectric and electrical behaviors of Co-Zn ferrite material in detail. The samples are prepared by solid state reaction method and the structural properties have been described utilizing high-resolution X-ray diffractometer (HRXRD). Both temperature and frequency dependence of dielectric constant has been reported, also, the temperature and frequency dependence of dielectric $\tan \delta$ loss have been studied thoroughly.

4.2 Synthesis

Molybdenum substituted cobalt-zinc ferrite having general chemical equation $\text{Co}_{0.65}\text{Zn}_{0.35}\text{Fe}_{2-x}\text{Mo}_x\text{O}_4$ ($x=0.0, 0.1, 0.2$) have been prepared by the conventional ceramic method/solid state reaction method. The stoichiometric amount of high purity (99.99%) Co_3O_4 , ZnO , Fe_2O_3 and MoO_3 compounds were weighed and mixed appropriately. The mixture was ground utilizing an agate mortar and pestle for 3-4 hours in a volatile medium of exceedingly unadulterated (99.99%) acetone. The fine dried powder was calcined in air at 1100°C for 24 hours in a high-quality alumina crucible in a PID controlled tube furnace followed by furnace cooling. This procedure was repeated 2-3 times with intermediate

grinding. At last, the ground fine powder was mixed with little amount of 5% PVA (polyvinyl alcohol) as a binder. To pelletize the sample, a small amount of powder is kept in a die and punch and pressed by a hydraulic press with pressure $\sim 20 \text{ ton/cm}^2$. The pellets were then sintered at 1200°C for 36 hours in air followed by the furnace cooling. Now, the surface of pellets is smoothed using a fine sandpaper and coated with Silver (Ag) paste for electric, dielectric measurements. The hierarchy showing step by step synthesis procedure is displayed in Fig. 4.1.

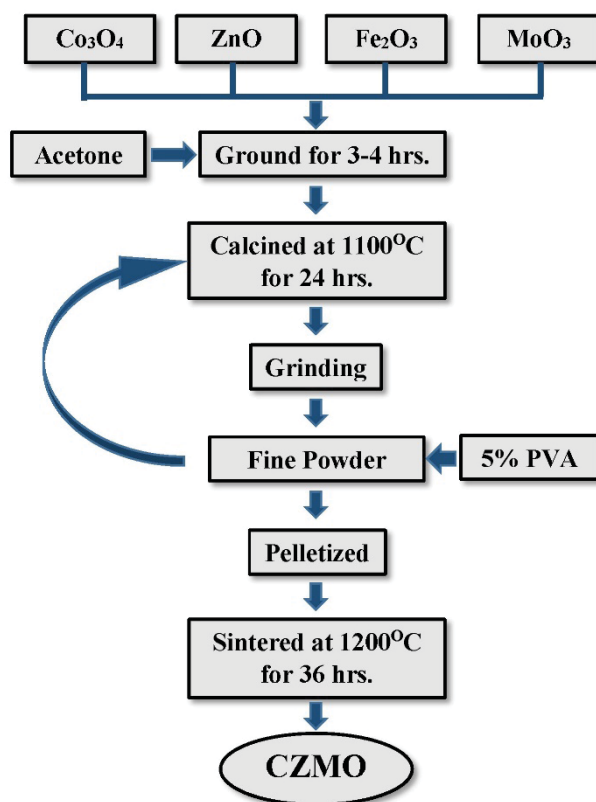


Fig. 4.1. Flow chart of CZMO synthesis process via ceramic method.

4.3 Structural properties

The high-resolution X-ray diffraction (HRXRD) pattern of $\text{Co}_{0.65}\text{Zn}_{0.35}\text{Fe}_{2-x}\text{Mo}_x\text{O}_4$ samples utilizing Cu-K α radiation is appeared in Fig.4.2. From the XRD pattern, it is evident that each samples are exceedingly crystalline and does not exists any contamination phase peak at the background level. It additionally proposes that the samples have exact cubic inverse spinel structure having $Fd3m$ [211] space group which has been validated from JCPDS database (Card No. 22-1086). The HRXRD data is taken over a 2θ range of 20° - 70° . The sharp diffraction maxima appeared relating to the lattice planes having (hkl) value (220), (311), (222), (400), (422), (511) and (440). The most extreme intensity has been seen relating to the reflection from (311) plane.

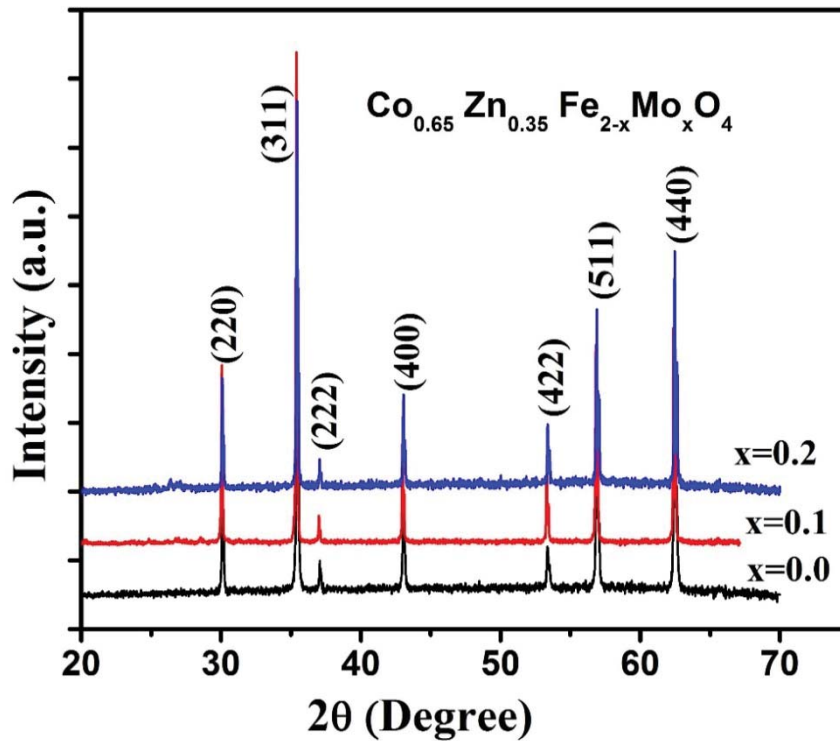


Fig. 4.2. High resolution X-ray diffraction pattern of $\text{Co}_{0.65}\text{Zn}_{0.35}\text{Fe}_{2-x}\text{Mo}_x\text{O}_4$ for $x=0.0, 0.1$ and 0.2 . The individual peaks are leveled with Miller indices corresponding to the plane of diffraction.

The lattice constant of the samples are computed utilizing the equation [82]

$$a = \frac{\lambda}{2} \sqrt{\left[\frac{h^2 + k^2 + l^2}{\sin^2 \theta} \right]} \quad (4.1)$$

where λ represents the wavelength of X-ray and (hkl) displays the Miller indices of the relating plane. The estimated lattice constant relating to (311) plane for pure Co-Zn ferrite is $\sim 8.3869\text{\AA}$. It is seen that the lattice constant gradually increases with increment in the concentration of Mo substitution [Table 4.1]. The grain size is calculated by utilizing the Debye-Scherrer's equation as [212]

$$D = \frac{0.9\lambda}{\beta \cos \theta} \quad (4.2)$$

where β is FWHM (full width at half maxima). The mean grain size is found to be increases with increasing Mo content. The variation of lattice constant and grain size is demonstrated in Fig. 4.3 and its inset respectively.

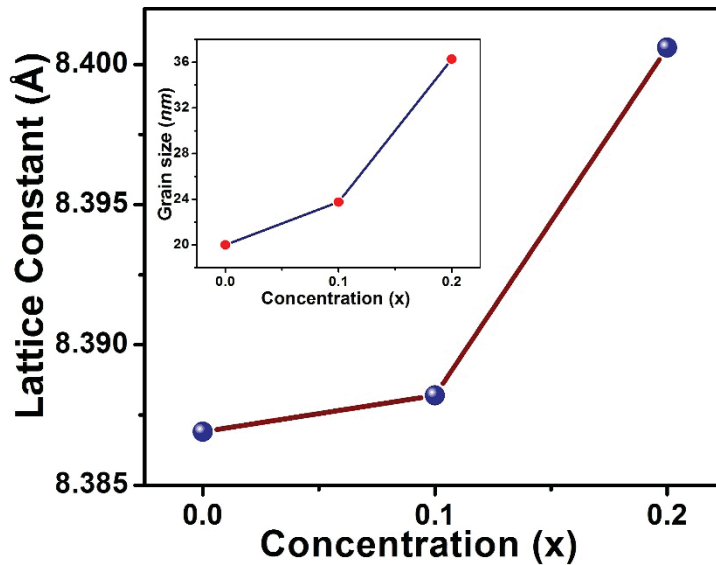


Fig. 4.3. Variation of lattice constant with Mo concentration. The inset shows the change in grain size with increasing Mo content.

The density of the samples is computed by using the equation

$$\rho = \frac{8M}{N_A a^3} \quad (4.3)$$

where M represents the molecular weight of the compound, N_A measures the Avogadro's number and the lattice constant is a , evaluated from the XRD data. The density increases with Mo doping content. The figured parameters are recorded in Table.1.

Table 4.1. Quantitative analysis of XRD pattern of Mo doped Co-Zn ferrite samples.

Mo concentration (x)	Lattice constant (a) in Å	Grain size (d) in nm	Strain	Density in gm/cc
0.0	8.3869	20.00	0.0118	5.33
0.1	8.3882	23.75	0.0099	5.39
0.2	8.4006	36.21	0.0065	5.51

4.4 Dielectric properties

4.4.1 Dielectric constant

The dielectric constant of a sample of ferrite may be estimated by utilizing the accompanying condition as [60]

$$\epsilon_r = \frac{C_0 d}{\epsilon_0 A} \quad (4.4)$$

where C_0 represents the air capacitance, 'd' is the thickness and 'A' is the area of the pellet and ϵ_0 is the free space permittivity.

The temperature reliance of dielectric constant of CZMO ($x= 0.0, 0.1, 0.2$) in various frequencies is delineated in Fig. 4.4. The curves recommend that there is a significant increment of dielectric constant temperature. The insets of the figure exhibit the amplified some portion of the curves. The dielectric constant of ferrite material is generated from four kinds of polarization, viz., interfacial polarization, electronic polarization, dipolar polarization and ionic polarization.

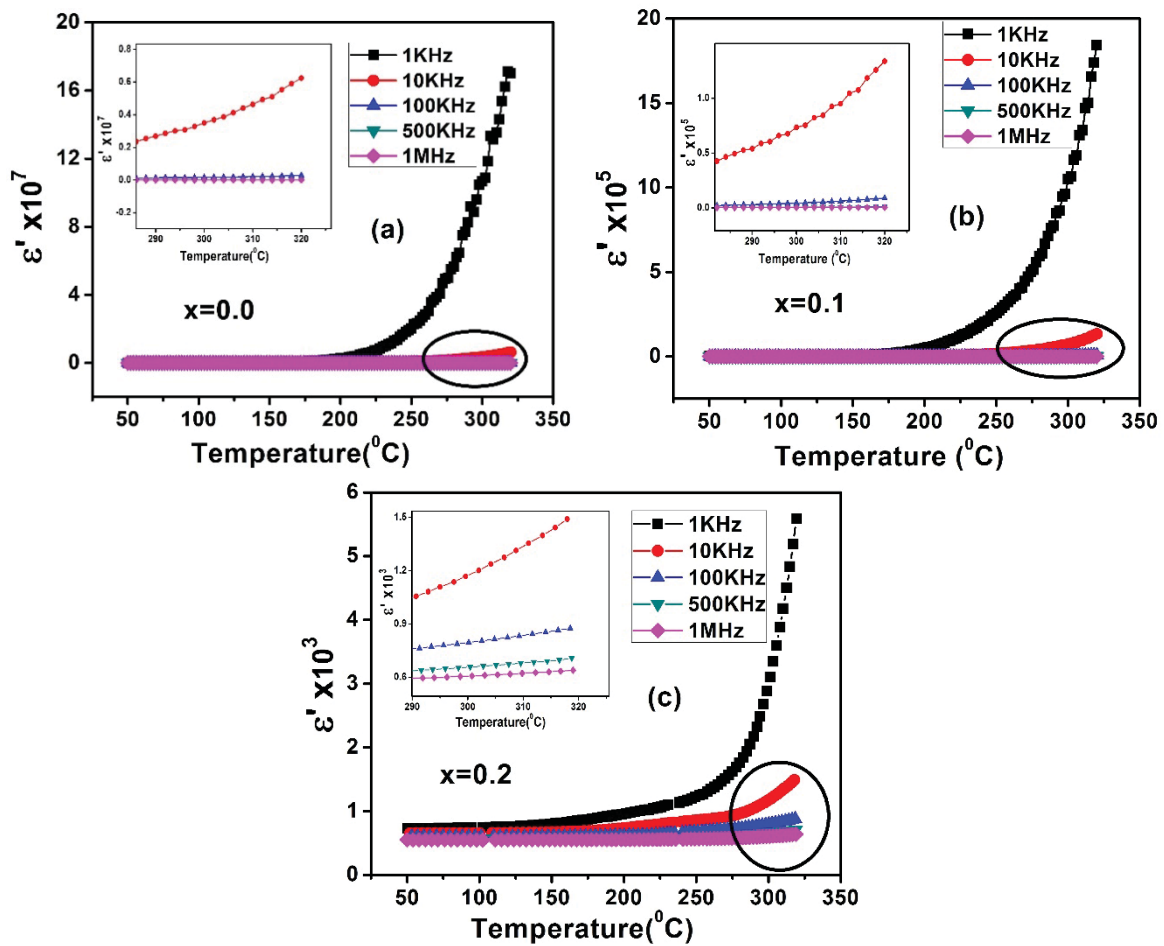


Fig. 4.4. Variation of dielectric constant with temperature at different frequencies of CZMO with (a) $x=0.0$, (b) $x=0.1$ and (c) $x=0.2$. The insets show the magnified portion of the curve.

Chapter 4

At lower frequency the dipolar and interfacial polarization are prevalent and both are temperature dependent. Interfacial polarization emerges because of the gathering of charge carriers at the grain boundary. The polarization in ferrite is like the conduction procedure which may be clarified based on the electron hopping mechanism. In cobalt-zinc ferrite as because of the exchange of electron between the ions, e.g., Fe^{2+} - Fe^{3+} , Co^{2+} - Co^{3+} , and Zn^{2+} - Zn^{3+} in two adjacent crystallographic sites, there is a local displacement of electrons in the applied field direction prompting the polarization [59].

It is understood that the dielectric behaviors of ferrites rely upon few factors, for example, cation distribution, preparation technique, structural homogeneity, sintering temperature, grain size, density, porosity and so on. The temperature variation of dielectric constant might be elucidated based on thermally assisted relaxation mechanism [127]. At lower temperature, the thermal energy isn't adequate to increase the mobility of the charge carrier and most of the time, the carriers can't arrange themselves with regard to the field direction. However, at higher temperature, the measure of thermal energy is large enough to enhance the hopping rate and therefore the charge carrier mobility so that they will be able to effortlessly order themselves at the direction of applied field. This enhances their commitment to polarization which prompts increment in the dielectric constant of the materials. The dielectric constant is maximum at low frequency (1 kHz) for every samples and diminishes with increasing frequency.

The complex dielectric constant may be communicated as

$$\varepsilon^* = \varepsilon' + i\varepsilon'' \quad (4.5)$$

;where the primary term represents the real part of dielectric constant which portrays the amount of energy stored and the last term is the imaginary part which depicts the amount of energy dissipation. The variation of both real and imaginary part of the complex dielectric constant is appeared in Fig.4.5. It is observed that every curves display the dielectric dispersion where both ϵ' and ϵ'' diminishes with increment in frequency. At lower frequency the dielectric constant diminishes sharply but when the frequency increases the decreasing rate turns out to be very low and becomes nearly constant at very high frequency. The dielectric dispersion proposed the critical enrichment of dielectric constant of Co-Zn ferrite because of Mo doping. At low frequency, the high estimation of dielectric constant is a direct result of the commitment of an extensive variety of polarization, for example, ionic, electronic, orientation and dipolar polarization so forth.

The high estimation of dielectric constant of the samples might be clarified based on the charge carrier hopping between the ions, e.g., $\text{Fe}^{2+} \leftrightarrow \text{Fe}^{3+}$, $\text{Co}^{2+} \leftrightarrow \text{Co}^{3+}$, $\text{Zn}^{2+} \leftrightarrow \text{Zn}^{3+}$ and $\text{Mo}^{2+} \leftrightarrow \text{Mo}^{3+}$ ions, with the goal that the electric dipoles adjust themselves towards the direction of the external ac field. The dielectric constant enhanced with increment in Mo concentration in light of the fact that the dielectric constant in ferrite relies upon the quantity of Fe^{2+} ions which can be polarized easily in comparison with Fe^{3+} ions. In Co-Zn ferrite with inverse spinel structure, the B-site holds the Co^{2+} ions, Zn^{2+} ions and half of Fe^{3+} ions whereas, the rest of Fe^{3+} ions involves in the A-site. The Co^{2+} and Zn^{2+} ions create the p-type carriers, i.e., holes while, Fe^{2+} , Fe^{3+} and, Mo^{3+} ions offers ascend to make n-type carriers, i.e., electrons. Therefore both electrons and holes are resides in the B-site and electrons alone, are the carrier in A-site. When the frequency increases the polarization

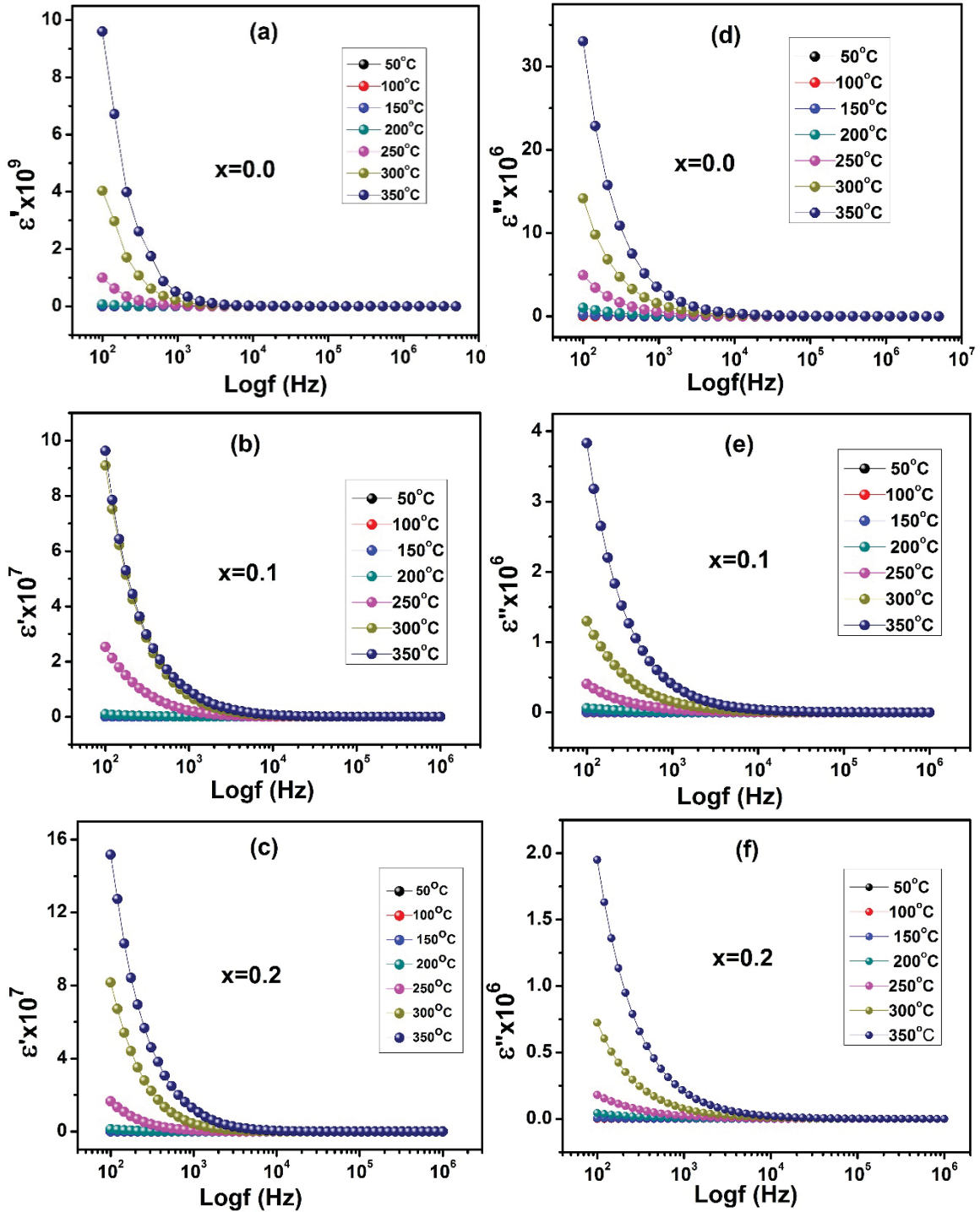


Fig. 4.5. The frequency dependence of the real part of dielectric constant of CZMO ferrites with (a) $x=0.0$, (b) $x=0.1$ and (c) $x=0.2$. The frequency dependence of imaginary part of dielectric constant of CZMO with (d) $x=0.0$, (e) $x=0.1$ and (f) $x=0.2$

decreases and attain a constant value because of the fact that after a specific frequency the hopping of electron can't pursue the applied ac field. Additionally at high frequency orientation polarization diminishes quickly as it needs much time compared to the ionic and electronic polarization and attains a constant value, describing the main contribution of interfacial polarization. Subsequently both ϵ' and ϵ'' diminishes at high frequency.

The dielectric dispersion mechanism in ferrite with a distinct relaxation time might be characterized by the Debye relation as [209]

$$\epsilon^*(\omega) = \epsilon'(\omega) + i\epsilon''(\omega) = \epsilon_{\infty} + \frac{\epsilon_s - \epsilon_{\infty}}{1 + i\omega\tau} \quad (4.6)$$

;where ϵ_s and ϵ_{∞} are the low and high frequency estimation of ϵ' , respectively, ω shows the angular frequency and τ represents the relaxation time. Be that as it may, we couldn't fit the curves according to the above relation. The dielectric relaxation values may be best fitted with the modified Debye relation expressed as [213]

$$\epsilon^*(\omega) = \epsilon'(\omega) + i\epsilon''(\omega) = \epsilon_{\infty} + \frac{\epsilon_s - \epsilon_{\infty}}{1 + (i\omega\tau)^\alpha} \quad (4.7)$$

;where α represents the width parameter and the estimation of α lies in the vicinity of 0 and 1. This perception uncovers that the relaxation mechanism is non-Debye type in the investigating ferrite samples. The frequency reliance of dielectric constant likewise propose that the dispersion is because of Maxwell-Wagner interfacial type polarization in agreement with Koop's phenomenological theory [73]. The model recommends that the ferrite comprises of two layers. One is a well-conducting layer, called the grain and another is a poor conducting layer, called the grain boundary. The grains are more active at high frequency, on the other hand the grain boundaries are active at low frequency. This is like

our perception of dielectric dispersion in the present sample. At a specific frequency, the electrons in the grain gathered at the grain boundary site as the grain boundary have high resistance. This conglomeration of electrons prompts make the space charge and thus the space charge polarization. As the temperature expands, more electrons are gotten together at grain boundary site bringing about an expansion of both polarization and dielectric constant. In any case, when the frequency raises the electrons have less time to arrange at the field direction and at a hopping frequency, the electrons basically can't take after the AC field bringing about a quick abatement of dielectric constant.

4.4.2 Dielectric loss tangent

The dielectric loss tangent can be described as

$$\tan \delta = \frac{\epsilon''}{\epsilon'} \quad (4.8)$$

;where δ is the loss angle, ϵ' is the real part and ϵ'' is the imaginary part of dielectric constant. The temperature reliance of $\tan \delta$ with various frequencies is appeared in Fig. 4.6 for CZMO with various doping content of Mo. It suggests that the $\tan \delta$ loss increases monotonously with temperature. Two peaks came into view related to the maximum $\tan \delta$ for $x=0.1$ as displayed in Fig. 4.6(b).

The peaks propose that with rise of frequency the peak shifted to the higher temperature showing the thermally activated relaxation mechanism. The condition for maximum dielectric loss of a ferrite sample is

$$\omega\tau = 1 \quad (4.9)$$

;where $\omega = 2\pi f$.

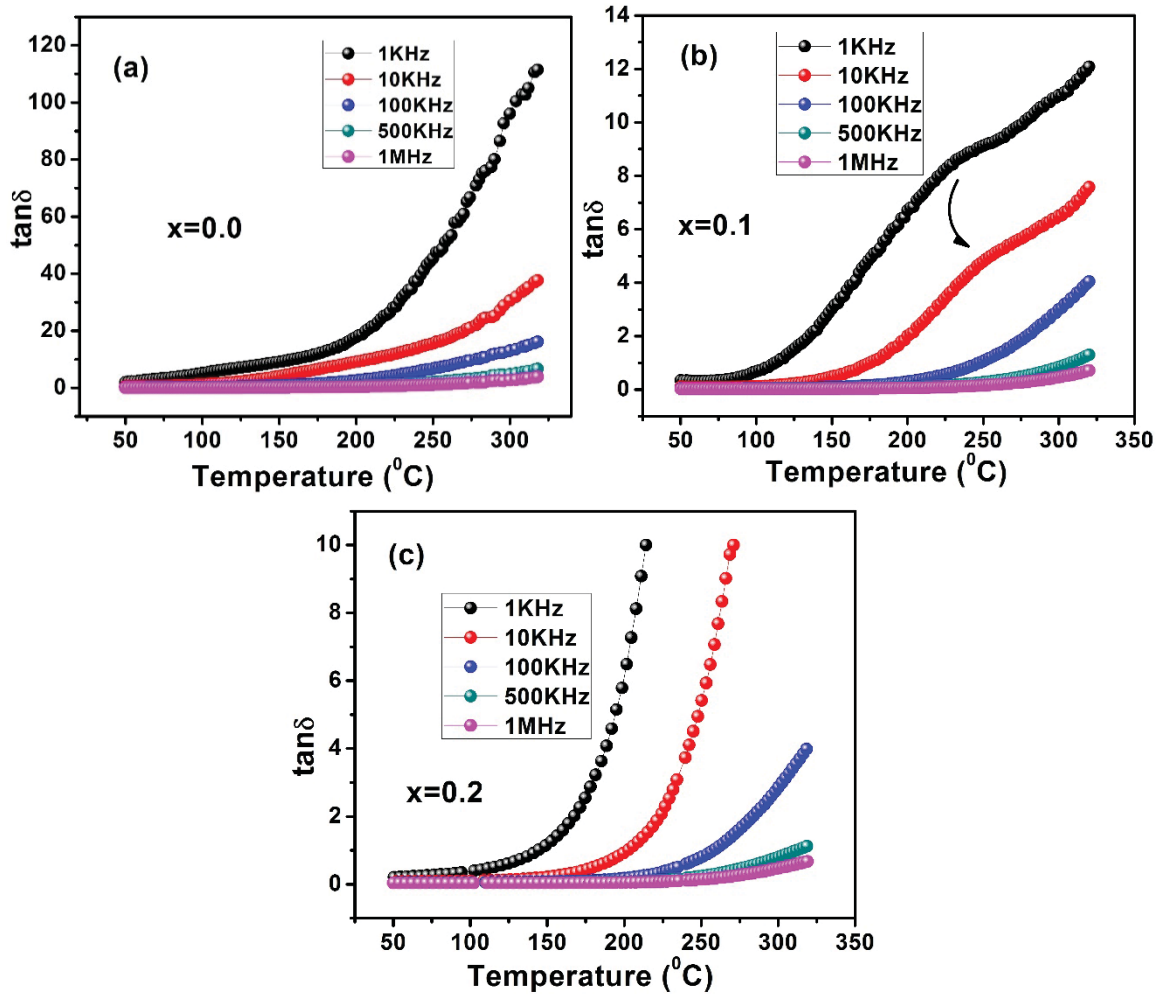


Fig. 4.6. Variation of dielectric loss with temperature of different samples. The arrow shows the shifting of $\tan \delta$ peaks.

The relaxation time τ relies upon the jumping probability per unit time 'P' as

$$\tau = 1/2P \quad \text{or,} \quad \omega_{max} = 2P \quad (4.10)$$

The shifting of peaks to high temperature with increment in frequency propose that the jumping probability enhances with increment in frequency. At high temperature the rapid increment of $\tan \delta$ as a result of the contribution of conductivity. The connection between the dielectric loss tangent and conductivity can be shown as [214]

$$\tan \delta = \frac{\sigma}{2\pi f \epsilon_0 \epsilon'} \quad (4.11)$$

where the conductivity is σ , f represent the frequency of ac field, ϵ_0 is the permittivity in free space and ϵ' illustrate the real part of the dielectric constant. The above condition demonstrates that the dielectric loss tangent is specifically relative to the conductivity. As the temperature builds the number of charge carrier increases expeditiously, therefore, the conductivity increments dramatically and consequently the loss tangent.

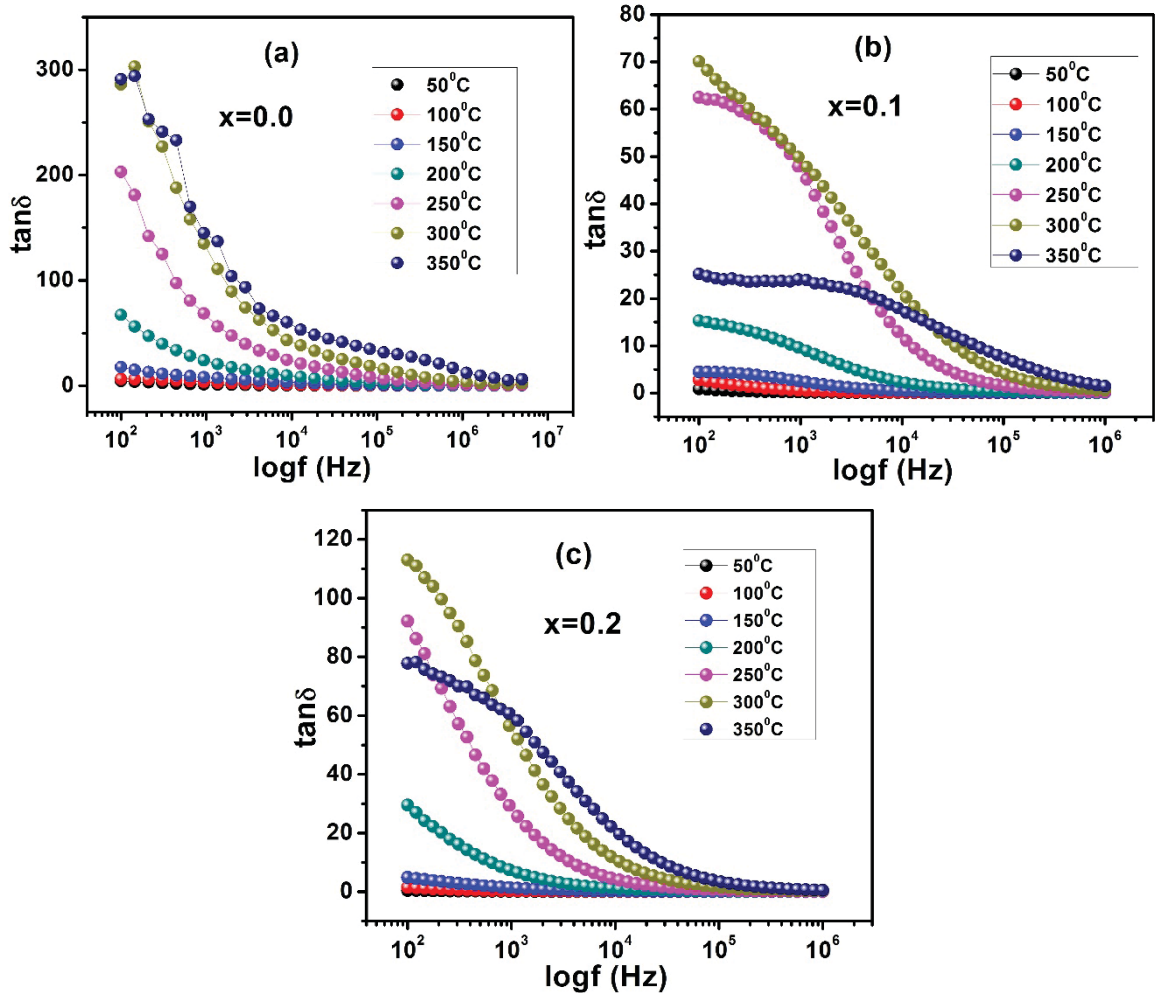


Fig. 4.7. The frequency variation of $\tan \delta$ loss of CZMO for $x=0.0, 0.1$ and 0.2 samples.

Fig. 4.7 portrays the variation of loss tangent with frequency in various temperature. The curves reveals that the loss tangent have the identical dispersion as in the dielectric constant. Dielectric loss emerges when the polarization lags behind the applied field and this should be due to the grain boundary effect, defects and impurity in the crystal [62]. The density of the material is additionally accountable for the variety of $\tan \delta$ [60]. The highly porous samples have low density which brings about low dielectric constant and high losses. At low frequency the high estimation $\tan \delta$ compares to the high resistivity of grain boundary.

Hence, much energy is needed for electron hopping, results in high energy loss. But at high frequency very feeble amount of energy is needed results in little amount of energy loss and small resistivity.